Journal of Magnetic Resonance **141,** 197–206 (1999)
Article ID jmre.1999.1901, available online at http://www.idealibrary.com on IDEAL®

Beyond *k*-Space: Spectral Localization Using Higher Order Gradients

Rolf Pohmann, Eberhard Rommel, and Markus von Kienlin

Department of Biophysics, University of Würzburg, Würzburg, Germany

Received December 18, 1998; revised July 29, 1999

Chemical shift imaging (CSI) often suffers from the inconvenient shape of its spatial response function (SRF), which affects both localization and signal-to-noise ratio. Replacing the magnetic field gradients for phase encoding by higher order magnetic fields allows a better adjustment of the SRF to the structures in the sample. We combined this principle with the SLOOP (spectral localization with optimal pointspread function) technique to simultaneously obtain spectra from several arbitrarily shaped compartments within a sample. Linear combinations of the fields of the shim coils are used to generate the pulsed fields for phase encoding. Their shapes are matched to the given sample geometry by numerical optimization. Using this method, spectra from a phantom were obtained that show a higher signal-to-noise ratio and a strongly reduced contamination compared to an equivalent CSI experiment. © 1999 Academic Press

Key Words: **localized spectroscopy; CSI; SLOOP; *k*-space; higher order gradients.**

INTRODUCTION

For almost 50 years, NMR spectroscopy has played an important part in chemical and biological research. Many biological and medical applications require spatially resolved spectra from different regions of the sample. This is often achieved with chemical shift imaging (CSI), which allows simultaneous acquisition of localized spectra across the whole sample with the aid of pulsed field gradients. They generate magnetic fields with a linear spatial dependence, which serve to encode the spatial information (*1, 2*). Localized spectroscopy often suffers from its long duration and from a low signal-to-noise ratio. Both factors impose strong limitations on the number of voxels that can be observed in a CSI experiment. Furthermore, the inconvenient shape of the spatial response function causes high contamination of the spectrum of one voxel by the signal of others. This effect can heavily deteriorate the results, in particular in experiments with relatively few phase encoding steps and a low spatial resolution. Several alternative techniques have been developed to improve the localization of spatially resolved spectra. They either apply optimized *k*-space sampling schemes (*3–5*) or use prior knowledge about the structure of the sample to obtain improved spatial response functions from either rectangular voxels (*6*) or from volumes with shapes that are adjusted to the sample geometry (*7–9*). The latter methods also improve the sensitivity of the experiment by maximizing the volume of each voxel.

While all these techniques use conventional phase encoding, we now have extended SLOOP (Spectral localization with optimal pointspread function (*8*)) to introduce a new way to achieve spatial resolution: Instead of only using constant gradients with a linear dependence of the magnetic field on space, we apply fields with a wider variety of shapes that are optimized for the geometry of the sample. For experiments with a low spatial resolution, a better spatial response function can be obtained by this more flexible way to encode the spatial information.

So far, pulsed magnetic fields with other than linear spatial dependence have mainly been used for volume selection. Most of these techniques apply quadratic field shapes (*10–13*). Our current implementation of the SLOOP^N technique (SLOOP using Nth order gradients (*14, 15*)) uses the shim coils to generate the desired magnetic field shapes and thereby obtains spectra with an improved localization and sensitivity compared to CSI experiments.

SLOOP^N can be beneficial for experiments in which spectra from only a small number of large voxels are desired. This applies in particular to situations where a low SNR only allows for a large voxel size, but it can also be of interest when the signal is high enough to already obtain a sufficient SNR with a very small number of phase encode steps. SLOOP^N employs pulsed higher order gradient fields during free precession delays to obtain a phase modulation with a nonlinear variation in space. Such a nonlinear phase encoding can also be obtained applying RF pulses in the presence of gradient fields. The field of potential applications of SLOOP^N thus is similar to that of methods that use tailored pulses for volume selection, such as RF-phase encoding (*16*), Hadamard imaging (*17*), or pinwheel pulses (*18*).

PRINCIPLE

The main difficulties of many localized spectroscopy experiments are the low concentration of the examined metabolites and the low sensitivity of the observed nuclei. They allow only for a crude spatial resolution in a tolerable duration. The results then are strongly affected by the inconvenient spatial response function (SRF) of the Fourier technique: Because of the small fraction of *k*-space covered in the experiment, the signal of a voxel does not fully originate in that voxel; strong contribu-

1090-7807/99 $30.00

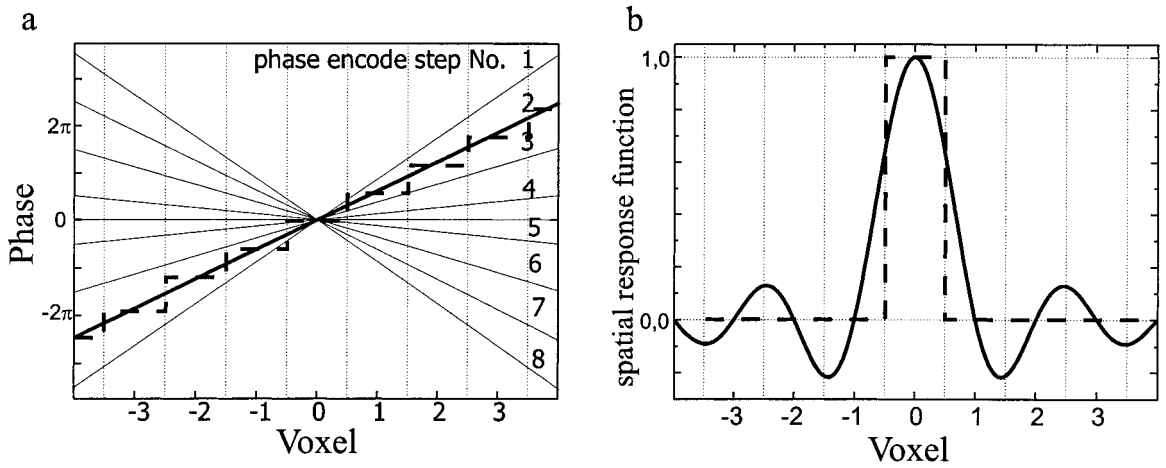

FIG. 1. A normal CSI experiment is performed by applying gradient pulses with varying strength before acquisition. The phase of the NMR signal then varies linearily with space, the slope depending on the strength of the phase encoding gradient. The straight lines in (a) show the phase variation in an eight-step CSI experiment. The result is a sinc-shaped spatial response function, shown in (b). An ideal, rectangular SRF could in principle be obtained by replacing the linear fields by step-like fields, which are constant inside each voxel but change fast at their borders. One such field is indicated by the dashed line in (a). To obtain the ideal SRF, eight such step-fields—each of them following one of the linear fields in normal phase encoding—are required.

tions come from surrounding tissue. The SRF, which displays the spatial origin of the signal of a pixel, is not square but a sinc-like function (Fig. 1b). This effect is responsible for two disadvantages of the CSI sequence: First, the wiggles of the sinc-function outside the desired voxel cause signal contamination from adjacent voxels, and second, not the entire magnetization within a voxel contributes to its signal. This latter effect results in an unavoidable signal loss of 13% per spatial dimension (*19*) due to phase dispersal in extended samples. For a three-dimensional experiment, this adds to a total loss of 34%.

The inconvenient shape of the SRF is caused by the gradients used for spatial encoding: They generate magnetic fields with a linear dependence on space, which induce a linear variation of the phase of the magnetization. The reconstruction algorithm then assigns for every phase encode step one value of the phase to each voxel. By doing so, it assumes a constant phase for the entire voxel. Due to the linear spatial dependence of the phase, however, only the center of the voxel has exactly that value. The localization of the outer parts of the voxel is imperfect, part of their signal appears in other voxels, causing contamination by undesired signal. Furthermore, the phase dispersal within the voxel causes the reduction of its signal amplitude.

These problems could in principle be avoided if the spatial encoding was performed with magnetic fields that are constant inside the voxels, but change rapidly at their borders. For a CSI experiment with eight phase encode steps, an example is shown in Fig. 1. The linear phase encoding fields are replaced by the same number of step-like fields (dashed line, only one of them is shown in Fig. 1a). They are constant within each voxel, being equal to the corresponding linear fields in the voxel centers. This way, the phase dispersal could be avoided and the SRF would have the ideal rectangular shape (Fig. 1b). This theoretical example shows that magnetic fields with other than linear shapes for phase encoding can improve the performance of spatially resolved spectroscopic experiments. When the structure of the sample is taken into account, a variety of field shapes may enhance the quality of the localization. Allowing more variable field shapes thus can improve both localization and sensitivity of the spectra. The most flexible way to generate the desired fields is to use a set of fields, the shapes of which form a basis system. By superimposing many of these higher order gradients, all possible field shapes can be generated. This allows a flexible adjustment of the geometry of the fields to that of the sample.

Possible field shapes, however, are restricted by the Maxwell equations, which do not allow arbitrary changes of the field strength inside the sample volume. Generating fields close to the optimal shapes is possible mainly for a small number of relatively large voxels. This kind of geometry is typical for SLOOP experiments (*7*, *8*, *20*, *21*), which allow the simultaneous acquisition of spectra from several arbitrarily shaped voxels. Since this technique is often used with a very small number of compartments, it is particularly well suited for being combined with higher order gradients. Furthermore, the SLOOP-reconstruction algorithm can easily be extended to cover higher order field shapes.

Magnetic fields are governed by the Maxwell equations. They state that the z component of all fields $\vec{B}$, generated by a coil outside the volume of interest, must observe the Laplace equation

$$\nabla^2 B_z = 0. \qquad [1]$$

All possible magnetic fields consist of linear combinations of the solutions to this equation. Neglecting those solutions that diverge at the origin and thus are not of interest in this case, it follows in the spherical coordinates r, ϑ, and φ:

$$B_{lm}(r,\vartheta,\varphi) \propto r^l Y_{lm}(\vartheta,\varphi). \quad [2]$$

Here, Y_{lm} are the real spherical harmonics, which are derived from the complex spherical harmonics by taking the real and imaginary part for the positive integer values of the parameters l and m, with $m \leq l$. For each pair of l and m there exist two functions Y_{lm}, which depend on either $\sin(m\varphi)$ or $\cos(m\varphi)$ (*22*).

A flexible way to generate arbitrary fields therefore is to use a set of coils which form magnetic fields with shapes that correspond to one spherical harmonic each. By adjusting the currents in each of these coils, any desired field shape can be generated as superposition of the individual fields. A set of coils which meets these conditions is present in every NMR-spectrometer: the shim coils (*23–25*). The consist of a set of usually between 10 and 20 coils that are used to homogenize the B_o field. Each of them corresponds to one of the functions in Eq. [2]. Using these field shapes for shimming ensures maximum flexibility of the fields, a high orthogonality, and a fast convergence toward the optimally homogeneous B_o field. A review on shimming, including a list of usually available shim coils with their mathematical expressions, can be found in (*26*). All these advantages can also be exploited for forming shaped magnetic fields for phase encoding. Shim coils usually are, however, not designed for fast switching and cannot be controlled by the pulse sequence. To use them for phase encoding, some modifications of the NMR instrument are required. They are described below.

RECONSTRUCTION

The reconstruction of a SLOOP^N experiment is derived from that of a regular SLIM/SLOOP experiment, which has been described in detail elsewhere (*7, 8, 20, 21*). Here, we will give only a short outline of the technique and its extension to include nonlinear phase encoding fields.

SLOOP^N exploits prior knowledge about the structure of the sample that, for instance, can be obtained from a high-resolution proton image. This image is used to define several compartments, the spectra of which are to be found. The experiment itself is similar to a CSI sequence, but with nonlinear phase encoding gradients. The reconstruction algorithm described below then finds the spectrum from each compartment. Exploiting the knowledge of the exact shape and position of a compartment to determine its spectrum, partial volume effects are avoided and contamination is reduced. Furthermore, the sensitivity is higher than in a normal CSI experiment, since the whole compartment volume contributes to each spectrum.

The experiment can be affected by all kinds of inhomogeneities inside each compartment that may cause contamination in the neighboring compartments. This effect can be minimized by optimally adjusting the shape of the SRF to the compartment. This is done by choosing an optimal set of phase encoding gradients. While in SLOOP this optimization is restricted to choosing the strengths of normal, constant gradients, SLOOP^N uses an additional degree of freedom by also varying the shapes of the encoding fields. Furthermore, the nonlinear fields reduce the intravoxel dispersion of the magnetization and thus cause an additional increase in sensitivity.

To get the signals of N compartments, an experiment with $M \geq N$ phase encode steps has to be performed. If $c_n(t)$ is the time-domain NMR signal per unit volume emanating from the nth compartment, the signal $p_m(t)$ acquired in the mth phase encode step is given by the sum of the signals from all compartments:

$$p_m(t) = \sum_{n=1}^{N} g_{mn} c_n(t), \quad m = 1, \ldots, M. \quad [3]$$

In a regular SLOOP experiment, the factor g_{mn}, that contains the influence of the phase encoding gradients, is given by

$$g_{mn} = \int_{\text{compartment } n} e^{-i\vec{k}_m\vec{r}}\,\mathrm{dV}, \quad [4]$$

where $\vec{k} = (\gamma/2\pi)\vec{G}\tau$ ($\vec{G}$ is the constant gradient used in a conventional experiment, τ the phase encoding time, and γ is the gyromagnetic ratio of the observed nucleus). In a SLOOP^N experiment, the constant gradients $\vec{G}$ are replaced by higher order gradients, the vector $\vec{k}$ is no longer defined and the k-space description of spatially resolved experiments is no longer valid. The higher order fields have to be taken into account when calculating the factor g_{mn}:

$$g_{mn} = \int_{\text{compartment } n} e^{-(\gamma/2\pi)\,B_z(\vec{r})\cdot\tau}\,\mathrm{dV}. \quad [5]$$

The integral is performed over the whole volume of the nth compartment. $B_z(\vec{r})$ describes the spatial variation of the magnetic field

$$B_z(\vec{r}) = \sum_i B_i(\vec{r}), \quad [6]$$

B_i being the individual magnetic fields generated by the I shim coils to form the total magnetic field B_z, which may vary freely (within the limits set by the Maxwell equations) over the sample volume. The sum is performed over all I shim fields used in the experiment. The g_{mn} factor can also be used to include further information about spatial variations in the parameters of the sample or the instrument, like B_1 inhomogeneities or T_1 differences, as described in (*20*). These extensions are not applied in our experiments.

The signals $c_n(t)$ can be recovered from the measured signals $p_m(t)$ by constructing the M-dimensional vector $\vec{P}_M$ and

the N-dimensional vector $\vec{C}_N$, which consist of the $p_m(t)$'s and the $c_n(t)$'s, respectively. With the $M \times N$ matrix **G,** whose elements are the g_{mn}, Eq. [3] becomes

$$\vec{P}_M(t) = \mathbf{G}\vec{C}_N(t). \quad [7]$$

This equation can be solved by finding the pseudoinverse (or, in the case of $N = M$ the inverse) **H** of **G,** for which **HG** = 1. **H** is a matrix of size $N \times M$, which can be found numerically by performing a singular value decomposition (SVD) (*27*).

Having found **H,** the time domain signals from the various compartments can be obtained with

$$\vec{C}_N(t) = \mathbf{H}\vec{P}_M(t). \quad [8]$$

To evaluate the performance of the experiment and to find the optimal phase encoding fields for every phase encode step, two criteria are defined, which assess the quality of the localization and the signal-to-noise gain for the given geometrical structure. The localization criterion describes the contributions of the SRFs of the other compartments to the signal of the examined one. The reconstruction algorithm ensures that the integral of the SRF of the nth compartment (SRF_n) over the volumes of all other compartments is zero. To evaluate the susceptibility to inhomogeneities, the integral over the absolute value of the SRF is taken:

$$L_n = \int_{\text{outside compartment } n} |SRF_n(\vec{r})| \mathrm{d}\vec{r}. \quad [9]$$

L_n describes the largest possible degree of contamination as a worst case criterion. A small value means a low degree of potential contamination in the signal of compartment n. The phase encoding fields thus must be chosen as to minimize this criterion.

The signal-to-noise efficiency of an experiment is assessed by a second criterion, which compares the SNR of the signal of one compartment to that of a hypothetical, ideal experiment, where no signal is lost because of phase dispersal inside the compartments. It can be calculated as

$$\frac{SNR_n}{SNR_{n,opt}} = \frac{1}{V_n \sqrt{\Sigma_m |h_{nm}|^2}}, \quad [10]$$

where SNR_n and $SNR_{n,opt}$ are the SNRs of the nth compartment in the real and the hypothetical experiment, respectively (*8*). V_n is the volume of the compartment and the h_{nm} are the matrix elements of **H** in Eq. [8]. This criterion must be maximized to achieve the highest possible sensitivity.

These two criteria are used to find the optimal values of the phase encoding fields for a given sample structure. This is done by a numerical optimization algorithm which minimizes the localization criterion, Eq. [9], and maximizes the sensitivity, Eq. [10], by varying the shim currents for each phase encoding step. Since the two criteria are often opposed, a compromise must be found. For this optimization, we used a simple Marquardt–Levenberg algorithm (*28*), which is susceptible to local minima. Local minima can in principle be avoided by applying a more sophisticated algorithm (such as "simulated annealing" (*29*)). Because of the high computational demands of those algorithms for the large number of parameters that must be optimized, they were not used in our calculations. We therefore cannot know whether we have found the optimal set of parameters, especially when a large number of phase encode steps or shim fields is used. To increase the probability of finding a good solution, the optimizations were repeated several times with different starting values and the best solution was retained.

INSTRUMENTATION

Experiments were performed on a BRUKER AMX-500 spectrometer with a field strength of 11.7 T and equipped with imaging gradients. This system is supplied with 17 shim coils. The instrumentation displayed in Fig. 2 was built to enable the use of these coils for pulsed phase encoding and to still be able to perform normal shimming. A table containing a list of amplitudes for each of the coils in every phase encode step is loaded into a personal computer, which is equipped with two 10-channel digital/analog converter cards (model AT-AO-10, National Instruments). One of their additional digital input channels is used for a trigger pulse from the spectrometer to synchronize the PC with the pulse sequence. A home-written computer program switches the output channels according to the values listed in the gradient table. The shape of the gradient pulses is generated by one of the D/A output channels and is used to form the pulse shapes by multiplication with the constant field amplitudes of each phase encode step. This allows a free adjustment of the waveform and the duration of the pulses as well as of the switching rate to minimize eddy currents. These signals are added to the constant voltage used for the normal shim currents by means of summation units in the shim amplifier. This procedure ensures that normal shimming is still possible. To allow fast pulsing, the bandwidth of the shim amplifier, which is usually small to avoid high-frequency variations of the shim currents, had to be increased to allow time constants of less than 1 ms.

Since Eq. [6] contains the spatial dependence of all the shim fields $B_i(\vec{r})$ throughout the sample, those fields first must be measured. This was done by performing a normal spin-echo imaging sequence on a homogeneous water sample, where a pulse into one of the shim coils is applied before, and a second, inverted one after the refocusing 180° pulse (Fig. 3b). Then, the same experiment is repeated, with an inverted sign of the shim pulses. By subtracting the phases of the two resulting images, a field map of the respective shim coil can be computed. It is vital that these images are acquired with the same

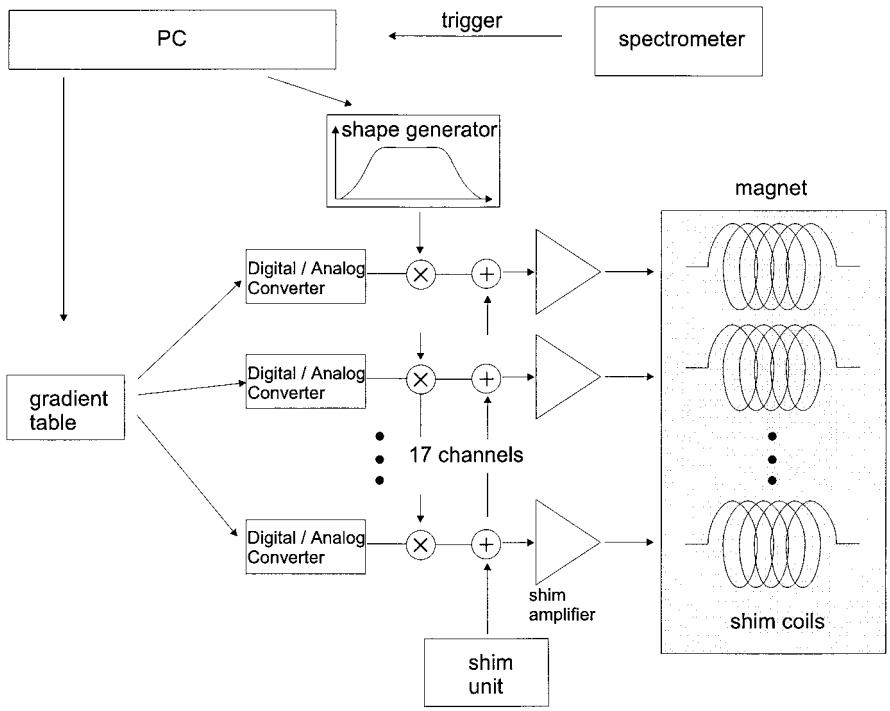

FIG. 2. The instrumentation used for performing phase encoding with the shim coils. An external PC stores the field strengths for every phase encode step. After receiving a trigger pulse from the spectrometer, the amplitudes of the higher order phase encoding gradients are read from a table, converted to analog values, multiplied by a waveform shape generator, and added to the constant shim currents. The bandwidth of the shim amplifiers is increased to allow rapid field changes.

timing (i.e., echo time, length, shape, and position of the gradient pulses) as the spectroscopic experiments, since switching the unshielded shim coils generates strong eddy currents, whose influence on the magnetic field has to be taken into account for the calibration. The measured field strengths of some of the shim coils are listed in Table 1.

Before the spectroscopic experiment is performed, the optimal values for all shim currents and phase encode steps must be found. Since this optimization depends on the geometrical structure of the sample, a proton image is taken, from which the necessary spatial information is extracted. An image segmentation is performed to define the compartments from which spectra are to be obtained. Then, the quality criteria defined at the end of the previous section are used to numerically determine the optimal phase encoding fields. The good B_1 homogeneity of the applied birdcage resonator in the plane used in the two-dimensional experiments allows to neglect corrections for B_1 inhomogeneities, which would require additional factors in Eq. [5], without severe degradation of the localization.

The spectroscopic experiments in two and three dimensions were performed with the pulse sequence of Fig. 3a. For the two-dimensional experiments, a slice-selective excitation pulse was applied in the presence of a constant gradient in slice direction, followed by a hard 180° refocusing pulse. Half echoes were sampled. For the three-dimensional experiment, the excitation pulse was replaced by a nonselective pulse and the slice gradient was omitted. The low field strengths of the shim coils, that are much weaker than normal imaging gradient coils, imply a rather long duration of the phase encoding gradients. To minimize eddy currents, a long rise time of 2.5 ms was used, the total phase encoding time τ was 20 ms. By splitting the phase encode gradient into two halves, one before and a second, inverted one after the refocusing pulse, the total echo time could be reduced. Nevertheless, an echo time of 50 ms was necessary because of the long phase encoding periods and to allow for decay of the eddy currents. The structural information from the proton images was then used to reconstruct the spectra from the various compartments with the aid of home-written IDL ("Interactive Data Language," RSI, Boulder, Colorado) routines.

To allow an evaluation of the new technique, CSI experiments with the same number of phase encoding steps (performed with the normal gradient coils) and identical timing were performed and their results were compared to those obtained with the SLOOP^N technique.

RESULTS

We performed two- and three-dimensional experiments using the SLOOP^N technique on a simple two-compartment phantom, consisting of tubes filled with water (inner tube) and lubrication oil (outer tube, Fig. 4). The water was heavily doped with copper sulfate to get a similar short T_2 in both

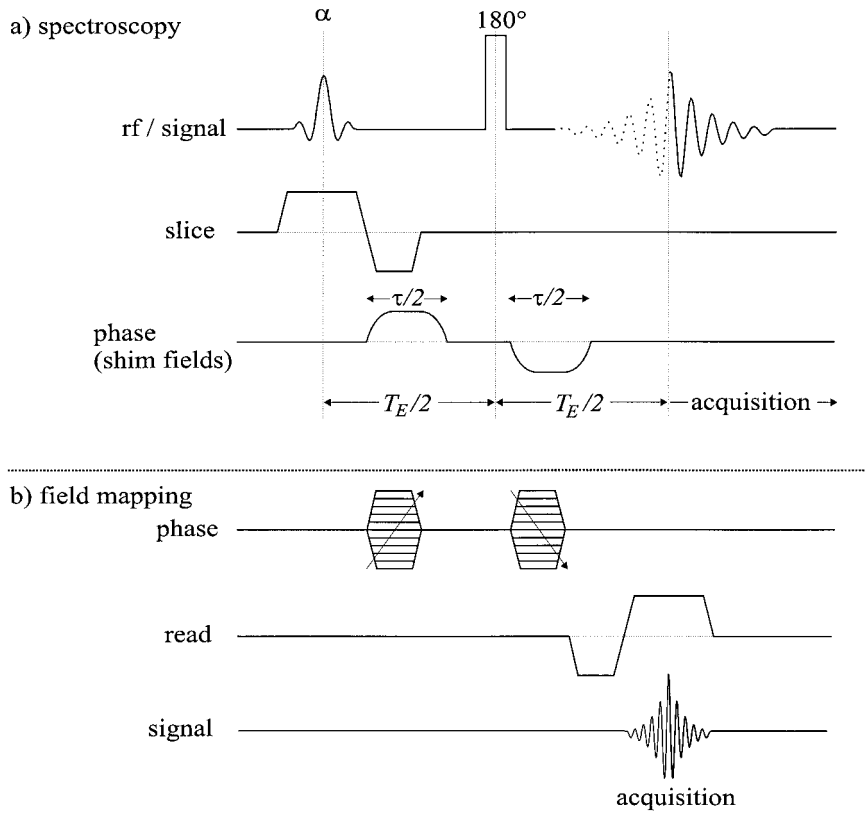

FIG. 3. The pulse sequence used for SLOOP^N is similar to that of a normal spin-echo CSI experiment, where the phase encode gradients are replaced by pulses into the shim coils. For three-dimensional experiments, the excitation pulse is nonselective and the slice gradient is omitted. All experiments were performed using a repetition time of $T_R = 1$ s, an echo time of $T_E = 50$ ms, and a phase encoding time of $\tau = 20$ ms. The 2D-experiment consisted of 16 phase encoding steps with four phase-cycled (EXORCYCLE) averages, the 3D experiment of 64 steps without averaging. All experiments thus took about one minute. Panel (b) shows the additional imaging gradients needed to measure the field maps of the shim coils.

compartments. The oil signal consisted of two lines from fat at 0.4 and 0.8 ppm, containing no additional contributions in the region of the water frequency (4.7 ppm). Signals from both compartments can therefore be distinguished clearly to detect contamination. A segmented image of the phantom was used to optimize the phase encode fields for a two-dimensional experiment with 16 phase-encode steps. Only six of the 17 available shim coils show considerable variation in the selected transversal plane and were used in the experiment. The field amplitudes found by the optimization algorithm are listed in Table 1. To be able to compare the SNR of the spectra, a low flip angle of about 1° was used. The slice thickness was 0.5 mm, a phase cycle (EXORCYCLE) required four averages.

The acquired signals were then reconstructed by the SLOOP^N algorithm. To compare the results to conventional methods, a normal CSI experiment with the same total number of phase encode steps ($N = 4 \times 4$, $FOV = 18$ mm) and identical other parameters was performed. Typical CSI spectra of both compartments can be seen in Fig. 4a. Especially the outer fat compartment shows a strong contamination by water signal and a low signal-to-noise ratio.

In the SLOOP^N spectra of the two compartments, Fig. 4b, the contamination by unwanted signals is almost completely suppressed. Furthermore, a strong gain in the signal-to-noise ratio is observed. In this case, SLOOP^N allows one to obtain much better results than the classical CSI sequence. The reason for this difference is shown in Fig. 5, which displays the SRF of the two experiments for the outer compartment: For both methods the absolute values of the SRF show significant contamination from the water compartment. The rapid phase changes in that compartment in the SLOOP^N experiment, however, ensure that the positive contributions from the water signal are exactly cancelled by negative contributions. Furthermore, the SRF of the SLOOP^N sequence shows that the entire volume of the oil compartment contributes to its signal, causing a much better signal-to-noise efficiency.

This result is confirmed by the quality criteria: For the SLOOP^N experiment, the localization criterion (Eq. [9]) for the outer compartment is 0.15, the sensitivity criterion (Eq. [10]) is 0.42. The corresponding values for the CSI experiment are 0.32 for localization and 0.15 for sensitivity. Both criteria thus agree with the improved results for the SLOOP^N sequence. Since B_0 and B_1 inhomogeneities as well as inaccuracies in the shim maps have not been considered in the reconstruction, the accuracy of the sensitivity criterion is limited, causing an only qualitative agreement with the measured SNR difference.

TABLE 1
Shim Fields Used in the 2D Experiment

Shim	x	y	$x^2 - y^2$	xy	xz^2	yz^2
$B_{max}/\mu T$[a]	13.7	47.0	8.6	13.9	47.0	9.2
pe-step	Percent of maximum amplitude[b]					
1	14.5	−0.538	−20.1	1.12	−3.77	19.8
2	15.8	0.147	−22.4	0.733	−3.72	−2.76
3	−8.17	0.758	−5.26	−2.37	2.91	−2.47
4	−1.37	−0.220	−1.00	−2.27	1.44	5.21
5	2.32	−0.318	6.99	1.17	−1.59	−4.50
6	2.62	−0.440	−0.147	0.465	−0.416	8.63
7	30.6	−0.733	25.3	1.25	−1.08	−3.55
8	−0.171	0.196	5.33	1.61	−1.22	−5.00
9	−19.6	−0.440	25.3	−1.71	5.97	−2.08
10	−15.1	−0.122	25.0	−1.08	2.81	−18.6
11	−12.3	0.856	25.1	−1.30	1.52	−6.87
12	−12.2	0.905	9.76	−1.54	6.09	3.28
13	−9.95	0.000	6.94	−1.03	3.67	5.00
14	0.538	−0.073	−0.538	0.269	−0.904	−10.4
15	13.4	0.000	−8.36	0.489	−5.33	6.43
16	9.56	−0.807	−4.77	−0.562	−2.40	7.04

[a] Maximum field strengths of the six shim coils used for the two-dimensional experiment as difference between maximum and minimum field values over the FOV of the 2D-experiment.

[b] Shim fields used in the 16 phase encode steps of the two-dimensional SLOOP^N experiment. The values are listed as percent of the maximum amplitudes, shown above. They are the results of numerical optimization.

The shape of the inner compartment is much better suited for CSI experiments: Here, the localization criterion for CSI is 0.48 and therefore better than for SLOOP^N, where it is 0.95. However, since the integral of the SRF over the volume outside of the compartment is zero for SLOOP^N, but not for CSI, the contamination of the SLOOP^N spectrum of this compartment is still considerably smaller than for that acquired by CSI. The sensitivity criterion furthermore confirms the higher SNR in the SLOOP^N experiment (0.61 for SLOOP^N, 0.39 for CSI).

For three-dimensional structures, the limitations on the field shapes that are imposed by the Maxwell equations allow only for a less accurate approximation of the optimal values. The effect can be seen in Fig. 6. It shows the results of a three-dimensional experiment on a similar phantom as before. Sixty-four phase encode steps were performed and compared to a $4 \times 4 \times 4$ CSI experiment ($FOV = 18 \times 18 \times 45$ mm^3). Twelve shim coils were used to generate the higher order phase encode fields. The optimization of the field shapes then implies to find a minimum in a 64×12 dimensional parameter space. Although the difference in the quality of the CSI and the SLOOP^N spectra is not as striking as in Fig. 4, the contamination is still significantly reduced and the SNR in the outer compartment is increased. These results suffer from the highly inhomogeneous B_1 field of the resonator over the large FOV, which was not considered in the reconstruction.

DISCUSSION

The results displayed in Figs. 4 and 6 demonstrate the possibility of using the new technique to improve the quality of localized spectra. However, its application for experiments on biological and medical systems is limited by several restrictions. The main limitation is imposed by Eq. [1]: All magnetic fields inside a coil are linear combinations of the spherical harmonics, Eq. [2]. They do not allow arbitrary changes of the magnetic field inside the volume-of-interest. This is demonstrated in Fig. 7: The step function necessary for the optimal CSI experiment depicted in Fig. 1 is expanded in 49 spherical harmonics. Obviously, even for such a low resolution, the result deviates only slightly from a linear field for a large part of the FOV. This shows that the necessary field shapes for a SLOOP^N experiment can only be generated for a small number of large voxels. For an increasing number of compartments, the performance of the new technique will slowly degrade and at last become equal to that obtained with normal, constant gradient fields. This can already be observed for the three-dimensional case (Fig. 6), where the geometrical limitations on the possible field shapes are much stricter than in two dimensions, resulting in a less drastic performance gain.

Additional problems are introduced when the spectrometer's shim coils are used to generate the necessary fields. They are not designed for fast switching and therefore are not shielded. Switching the fields on and off induces strong eddy currents in conducting parts of the magnet and instabilities of the generated field. These effects must be taken into account when calibrating the experiment: The maps of the shim coils must be acquired with exactly the same timing as that used in the experiment. However, to avoid varying magnetic fields while sampling the echoes, one must make sure that these eddy currents have decayed to a large extent before acquisition. The spacing between gradient pulse and acquisition therefore must be long, which implies long echo times. Furthermore, the field strengths are much smaller than those of normal imaging gradients (Table 1). The length of the gradient pulses consequently must be quite long. Both arguments lead to the echo time of 50 ms that was used in our experiments. Such a long echo time causes a strong T_2-weighting and signal loss. Furthermore, the accuracy of the desired field shapes is restricted by the small number of shim coils, which limits the number of spherical harmonics available to form the fields.

All problems that are caused by using the shim coils can be relieved by the construction of dedicated coils, which generate the magnetic fields necessary for one particular sample geometry. This is of course only worth the effort if a similar geometry is used in many experiments. The flexibility then is reduced as price for a higher degree of localization.

A last problem of the technique is finding the optimal field shapes for the different phase encode steps: We are using a numerical optimization algorithm which, since a high number of parameters must be adjusted, is quite lengthy and susceptible to being trapped by local minima. The optimization for the

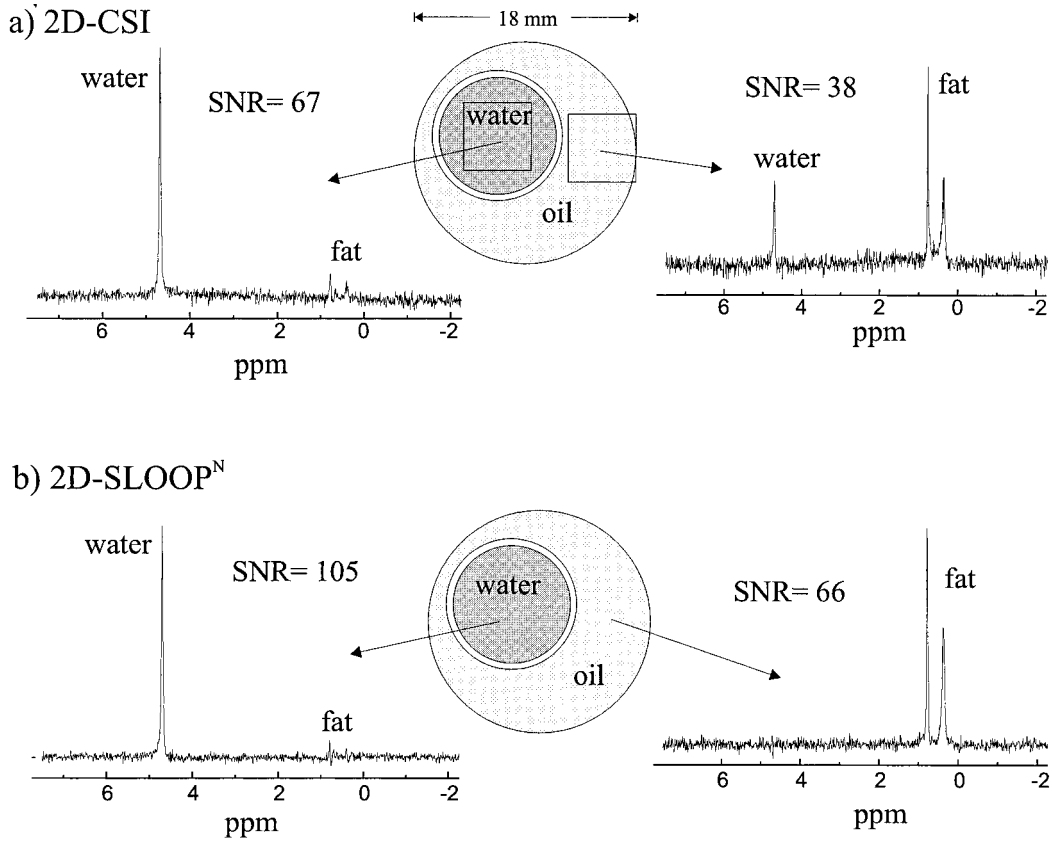

FIG. 4. Results of a two-dimensional experiment on a two-compartment phantom (center) filled with water (inside) and mineral oil (outside). (a) Results from a 4×4 CSI experiment, (b) results of a SLOOP^N experiment with the same number of phase encode steps. The 2D-SLOOP^N spectra show the improvement in localization, mainly for the outer compartment, where the unwanted water signal is completely suppressed. The SNR of the SLOOP^N spectra are improved by 57 and 74% for the inner and outer compartments, respectively. For the SLOOP^N experiment, linear combinations of six shim fields (x, y, $x^2 - y^2$, xy, xz^2, yz^2) were used for phase encoding (see Table 1).

three dimensional experiments of Fig. 6 took more than a day and had to be performed repeatedly with different initial parameter values. However, the best set of parameters has not necessarily been found for this experiment and even better results than those depicted in Fig. 6 might be possible. The use of SLOOP^N for routine applications would therefore require a

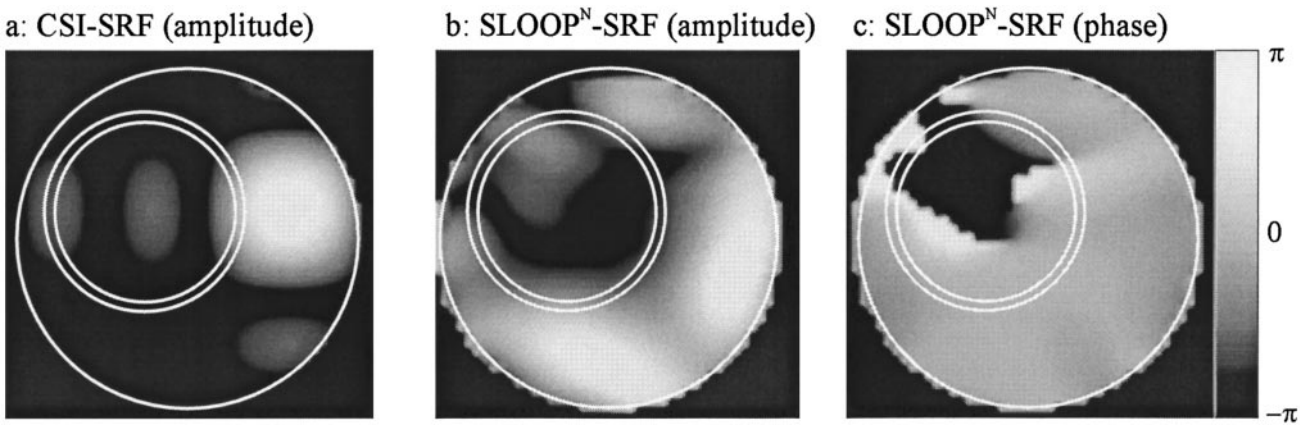

FIG. 5. Spatial response functions for the spectra from the oil compartment of the two-dimensional experiment of Fig. 4. For both sequences the absolute value is displayed, for SLOOP^N also the phase of the SRF is displayed (for CSI the SRF is purely real). The CSI experiment (a) shows the typical sinc-shaped SRF, causing contamination from the water compartment and a low signal-to-noise ratio. For the SLOOP^N-technique (b), the contamination from the water compartment is compensated by the (c) phase changes inside that compartment, which cause total cancellation of the unwanted signal. Inside the oil compartment no significant phase changes occur and the whole compartment contributes to the signal, resulting in a high SNR.

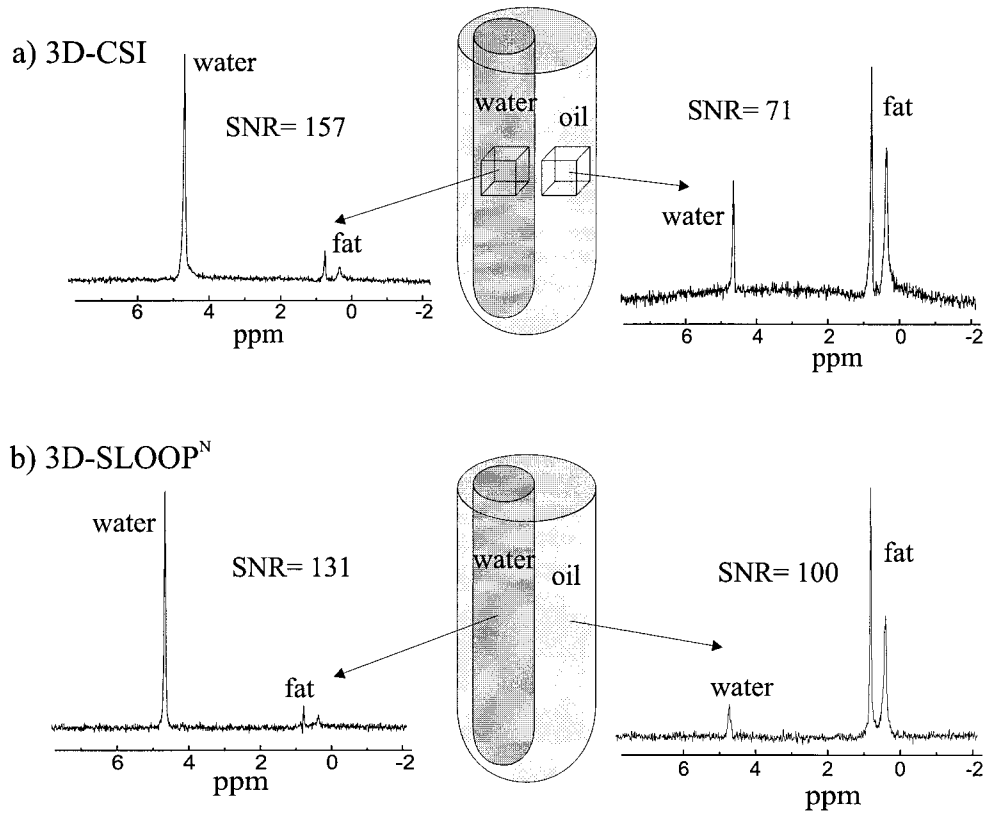

FIG. 6. Results from a three-dimensional experiment with (a) a $4 \times 4 \times 4$ CSI, and (b) a SLOOP^N experiment with 64 phase encode steps. Except for the SNR in the water spectrum, which is slightly reduced, the SLOOP^N spectra show significant improvements compared to those obtained by CSI. The shim fields applied for the 3D-SLOOP^N sequence were x, y, z, $x^2 - y^2$, z^2, xz, xy, xz^2, yz^2, z^3, z^4, and z^5.

better (if possible analytical) algorithm to find the optimal parameter values.

The results obtained with this technique show the capability of SLOOP^N to achieve a considerable gain in the quality of the localization of spatially resolved spectroscopic experiments with a low spatial resolution. The increased sensitivity and the reduced contamination allow better results in less time than is possible with conventional methods.

The approach presented here offers wider possibilities to adjust the experiment to the sample than conventional spatially resolved NMR techniques: While they apply the Fourier transform to obtain signals from a grid of rectangular voxels without inserting any additional information, newer methods use knowledge about the sample for the reconstruction to improve the localization. The data on which these algorithms are applied are in most cases obtained in conventionally performed experiments. A much better adjustment of the experiment to the sample is possible, when the *a priori* information is included not only in the reconstruction, but in the experiment itself. The most accurate way of doing so is by matching the shape of the fields for spatial encoding to the sample geometry. This is not possible with the constant gradients used normally for imaging, but higher order fields must be applied. Since they cannot be described with the *k*-space formalism, this concept exceeds the limits of *k*-space, using a more flexible localization scheme. The nonlinear fields thus allow maximum flexibility of the experimental parameters and leave the concept of *k*-space. While we have applied these principles to localized spectroscopy, there may also be other applications, where going be-

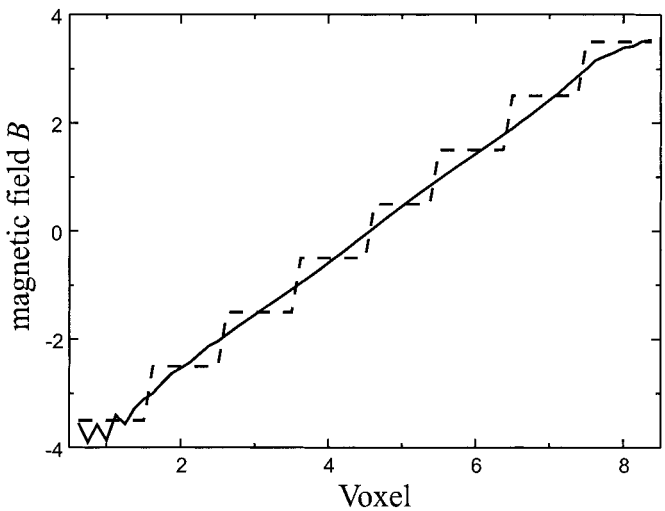

FIG. 7. A step function (dashed line) and its expansion in 49 spherical harmonics (solid line) by a least-squares algorithm. For a large part of the field of view, the result differs only slightly from a straight line, demonstrating the limited capability of the spherical harmonics to form arbitrary field shapes.

yond *k*-space allows one to better adjust the experimental parameters to the examined geometry.

ACKNOWLEDGMENT

This work was supported by the Deutsche Forschungsgemeinschaft, Grants Ki 433/2-2 and Ki 433/2-3.

REFERENCES

1. T. R. Brown, B. M. Kincaid, and K. Ugurbil, NMR chemical shift imaging in three dimensions, *Proc. Natl. Acad. Sci. USA* **79,** 3523–3526 (1982).
2. A. A. Maudsley, S. K. Hilal, W. H. Perman, and H. E. Simon, Spatially resolved high resolution spectroscopy by four-dimensional NMR, *J. Magn. Reson.* **51,** 147–152 (1983).
3. D. B. Twieg, The k-trajectory formulation of the NMR imaging process with applications in analysis and synthesis of imaging methods, *Med. Phys.* **10**(5), 610–621 (1983).
4. T. H. Mareci and H. R. Brooker, High-resolution magnetic resonance spectra from a sensitive region defined with pulsed field gradients, *J. Magn. Reson.* **57,** 157–163 (1984).
5. T. H. Mareci and H. R. Brooker, Essential considerations for spectral localization using indirect gradient encoding of spatial information, *J. Magn. Reson.* **92,** 229–246 (1991).
6. Z.-P. Liang and P. C. Lauterbur, A generalized series approach to MR spectroscopic imaging, *IEEE Trans. Med. Imaging* **10,** 132–137 (1991).
7. X. Hu, D. N. Levin, P. C. Lauterbur, and T. Spraggins, SLIM: Spectral localization by imaging, *Magn. Reson. Med.* **8,** 314–322 (1988).
8. M. von Kienlin and R. Mejia, Spectral localization with optimal pointspread function, *J. Magn. Reson.* **94,** 268–287 (1991).
9. M. Meininger, P. M. Jakob, M. von Kienlin, D. Koppler, G. Bringmann, and A. Haase, Radial spectroscopic imaging, *J. Magn. Reson.* **125,** 325–331 (1997).
10. S. Lee and Z. Cho, Localized volume selection technique using an additional radial gradient coil, *Magn. Reson. Med.* **12,** 56–63 (1989).
11. C. Oh, S. Hilal, Z. Cho, and I. Mun, New spatial localization method using pulsed high-order field gradients (SHOT: Selection with high-order gradient), *Magn. Reson. Med.* **18,** 63–70 (1991).
12. C. Rim, J. Ra, and Z. Cho, Radial scanning technique for volume selective ^{31}P spectroscopy, *Magn. Reson. Med.* **24,** 100–108 (1992).
13. E. Wu, G. Johnson, S. Hilal, and Z. Cho, A new 3D localization technique using quadratic field gradients, *Magn. Reson. Med.* **32,** 242–245 (1994).
14. M. von Kienlin, U.S. Patent 5509504, April 9th, 1996.
15. M. von Kienlin, Localized nuclear magnetic resonance spectroscopy using higher order gradients, *ZAMM* **4,** 28–31 (1996).
16. A. A. Maudsley, Fourier imaging using rf phase encoding, *Magn. Reson. Med.* **3,** 768–777 (1986).
17. G. Goelman, V. H. Subramanian, and J. S. Leigh, Transverse Hadamard spectroscopic imaging technique, *J. Magn. Reson.* **89,** 437–454 (1990).
18. C. J. Hardy, and P. A. Bottomley, ^{31}P spectroscopic localization using pinwheel excitation pulses, *Magn. Reson. Med.* **17,** 437–454 (1991).
19. A. A. Maudsley, Sensitivity in Fourier imaging, *J. Magn. Reson.* **68,** 363–366 (1986).
20. R. Löffler, R. Sauter, H. Kolem, A. Haase, and M. von Kienlin, Localized spectroscopy from anatomically matched compartments: Improved sensitivity and localization for cardiac ^{31}P-MRS in humans, *J. Magn. Reson.* **134,** 287–299 (1998).
21. M. Meininger, W. Landschütz, M. Beer, T. Seyfarth, M. Horn, T. Pabst, A. Haase, D. Hahn, S. Neubauer, and M. von Kienlin, Concentrations of human cardiac phosphorus metabolites determined by SLOOP ^{31}P NMR spectroscopy, *Magn. Reson. Med.* **41,** 657–663 (1999).
22. G. Arfken, "Mathematical Methods for Physicists," Chaps. 8.3 and 12.6, pp. 450 and 680–683, Academic Press, San Diego (1985).
23. M. J. E. Golay, Field homogenizing coils for nuclear spin resonance instrumentation, *Rev. Sci. Instr.* **29,** 313–315 (1958).
24. W. A. Anderson, Electrical current shims for correcting magnetic fields, *Rev. Sci. Instrum.* **32,** 241–250 (1961).
25. F. Romeo and D. Hoult, Magnetic field profiling: Analysis and correcting coil design, *Magn. Reson. Med.* **1,** 44–65 (1984).
26. G. N. Chmurny and D. Hoult, The ancient and honourable art of shimming, *Concepts Magn. Reson.* **2,** 131–149 (1990).
27. G. E. Forsythe, M. A. Malcolm, and C. B. Moler, "Computer Methods for Mathematical Computations," Chap. 9, Prentice Hall, New York (1977).
28. W. H. Press, B. P. Flannery, S. A. Teukolsky, and W. T. Vetterling, "Numerical Recipes in C—The Art of Scientific Computing," pp. 317–324, Cambridge University Press, Cambridge, UK (1988).
29. W. H. Press, B. P. Flannery, S. A. Teukolsky, and W. T. Vetterling, "Numerical Recipes in C—The Art of Scientific Computing," pp. 343–352, Cambridge University Press, Cambridge, UK (1988).